

ARTICLES

The Effect of Mutual Orientation on the Spectra of Metal Nanoparticle Rod–Rod and Rod–Sphere Pairs

Maryann Gluodenis and Colby A. Foss, Jr.*

Department of Chemistry, Georgetown University, 37th and “O” Streets NW, Washington, District of Columbia 20057

Received: November 16, 2001; In Final Form: May 13, 2002

A simple quasistatic treatment for the plasmon resonance spectra of nanoparticle rod–rod and rod–sphere pairs is presented. Spectra are calculated for gold particle pairs at different distances and mutual orientations. For rod–rod and rod–sphere pairs, the spectral changes that occur as a result of interparticle interaction are different for end-to-end (axial) and side-to-side (lateral) orientations. Axial interactions generally lead to a red shift of the most intense (longitudinal axis) plasmon resonance band. Lateral interactions usually lead to a blue shift of the main plasmon band. In general, lateral orientation yields more pronounced spectral changes than the axial case, especially as the aspect ratio of the rod member(s) increases.

Introduction

Analyte-induced aggregation of metal nanoparticles can result in a dramatic change in the extinction spectrum of the system, which in turn can be the basis of a signal useful for qualitative and quantitative analysis. Since the seminal paper by Mirkin, Letsinger, and co-workers,¹ the field of metal nanoparticle aggregation based bioassays has grown significantly.^{2–7}

In all of the work to date, metal nanoparticle based assays have utilized spherical nanoparticles, usually gold or silver. The reason for this is largely rooted in the fact that spherical nanoparticles are so readily available commercially and are also easy to prepare. In recent years however, numerous methods for preparing nonspherical metal nanoparticles have been developed, the most visible example being perhaps rodlike structures, which can be grown via electrochemical template synthesis^{8–13} or in bulk solutions containing special surfactants.^{14–16}

In this paper, we present the results of a theoretical study of the spectral consequences of the electromagnetic interaction of two metal nanoparticles in close proximity, in which at least one of these particles is rodlike. Because of the reduced symmetry of nonspherical particles, electromagnetic interactions of paired particles should depend not only on mutual separation distance, but also on *mutual orientation*. We are interested in determining how the mutual orientation of two particles in close proximity changes their plasmon resonance spectrum, relative to that of noninteracting members separated by large distances.¹⁷

For this study, we consider only particle pairs and utilize a simple quasistatic limit approach to calculate the extinction spectra of two interacting particles. In the quasistatic limit, the dimensions of the particles are assumed to be very small relative to the wavelength of the incident radiation. Rayleigh scattering theory and the Maxwell–Garnett and Bruggeman effective

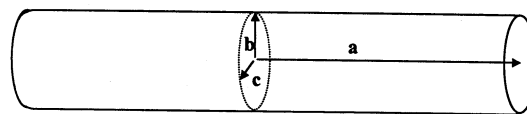


Figure 1. Schematic diagram of a rod and its semimajor axis a and semiminor axes b and c .

medium theories are all based on this assumption. Because these treatments are so often invoked to explain the experimental spectra of metal nanoparticle systems, it is useful to begin the discussion of paired nonspherical particles at this simple level.

Single Particle Scattering Theory

The optical properties of individual nanoparticles can be explained by the Clausius–Mossotti equation for particle polarizability^{18–20}

$$\alpha = \frac{4\pi\epsilon^0 ab^2}{3L_x} \frac{\epsilon_m - \epsilon_h}{\epsilon_m + \kappa\epsilon_h} \quad (1)$$

where ϵ_m and ϵ_h are the complex dielectric constants of the metal particle and its host medium, respectively, and ϵ^0 represents the vacuum permittivity. We assume that an ellipsoid of revolution is a reasonable representation for a rodlike particle; the relevant dimensions are thus its semimajor axis a and its semiminor axis b (see Figure 1).

The screening factor κ is dependent upon the particle shape and is related to the depolarization factor L_x via $\kappa_x = L_x^{-1} - 1$, where x denotes the semiaxis parallel to the incident field. For prolate ellipsoids of revolution, the general formula for calculating L along the axis of rotation is^{9,18}

$$L_a = \frac{1 - e^2}{e^2} \left(\frac{1}{2e} \ln \frac{1 + e}{1 - e} - 1 \right) \quad (2)$$

* To whom correspondence should be addressed. Current Address: Trex Enterprises Corporation, 3038 Aukele Street, Lihue, HI 96766. E-mail: cfoss@trexenterprises.com.

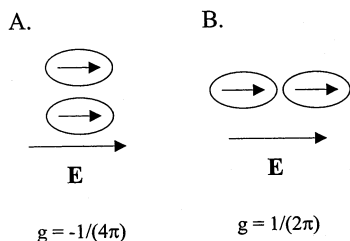


Figure 2. Schematic diagram showing the (A) end-to-end and (B) side-to-side alignments of two induced dipoles with the corresponding g factor.

where $e = (1 - b^2/a^2)^{1/2}$. The depolarization factor for an external field parallel to b can be derived from L_a via

$$L_b = (1 - L_a)/2 \quad (3)$$

The extinction cross section, C_{ext} , is easily calculated as the sum of the absorption and scattering cross sections via^{17,18}

$$C_{\text{ext}} = C_{\text{abs}} + C_{\text{sca}} \quad (4)$$

where C_{abs} and C_{sca} are obtained from the particle polarizability (eq 1) via^{18,19}

$$C_{\text{abs}} = k \text{Im}(\alpha) \quad (5)$$

$$C_{\text{sca}} = \frac{k^4}{6\pi} |\alpha|^2 \quad (6)$$

Interparticle Interactions

Kreibig and Vollmer²⁰ describe the quasistatic interaction of symmetric pair particles. To summarize, the electric dipole moment of each of the two particles is

$$\mu_1 = \epsilon_h \alpha_1 \mathbf{E}_1 \quad (7a)$$

$$\mu_2 = \epsilon_h \alpha_2 \mathbf{E}_2 \quad (7b)$$

where \mathbf{E}_1 and \mathbf{E}_2 are the electric fields experienced by particles 1 and 2, respectively. If the particles are far apart and non-interacting, \mathbf{E}_1 and \mathbf{E}_2 are equal to the local field, \mathbf{E} . However, if the particles are in close proximity, the electric field experienced by one particle is dependent on both the applied field \mathbf{E} and a field component arising from the second particle. Therefore, the fields at particles 1 and 2 can be defined as

$$\mathbf{E}_1 = \mathbf{E} + g \frac{\mu_2}{\epsilon_h \epsilon^0 d_{12}^3} \quad (8a)$$

$$\mathbf{E}_2 = \mathbf{E} + g \frac{\mu_1}{\epsilon_h \epsilon^0 d_{12}^3} \quad (8b)$$

where d_{12} is the center-to-center distance between the two particles and g is a factor that describes the pair orientation with respect to \mathbf{E} . If the two particles are aligned in the external field such that their induced dipoles are side-to-side, the factor g equals $-1/(4\pi)$.²¹ On the other hand, if the orientation of the pair is such that the induced dipoles interact end-to-end, $g = 1/(2\pi)$ (see Figure 2).

Substitution of eqs 7 into 8 and combination of eqs 8a and 8b leads to

$$\mathbf{E}_1 \left(1 - g^2 \frac{\alpha_1 \alpha_2}{d_{12}^6} \right) = \mathbf{E} \left(1 + g \frac{\alpha_2}{d_{12}^3} \right) \quad (9a)$$

$$\mathbf{E}_2 \left(1 - g^2 \frac{\alpha_1 \alpha_2}{d_{12}^6} \right) = \mathbf{E} \left(1 + g \frac{\alpha_1}{d_{12}^3} \right) \quad (9b)$$

Because the average polarizability of the pair of particles can be defined as

$$\frac{1}{2}(\mu_1 + \mu_2) = \epsilon_h \frac{1}{2}(\alpha_1 \mathbf{E}_1 + \alpha_2 \mathbf{E}_2) = \epsilon_h \langle \alpha \rangle \mathbf{E} \quad (10)$$

the combination of eqs 9 and 10 yields

$$\langle \alpha \rangle = \frac{\frac{1}{2} \left(\alpha_1 \left(1 + g \frac{\alpha_2}{d_{12}^3} \right) + \alpha_2 \left(1 + g \frac{\alpha_1}{d_{12}^3} \right) \right)}{1 - g^2 \frac{\alpha_1 \alpha_2}{d_{12}^6}} \quad (11)$$

Using this expression for particle pair average polarizability, along with eqs 4–6, we can calculate the extinction spectrum.

It should be emphasized that the above approach bases the electromagnetic interactions on point dipoles situated at the centers of each particle. Subtleties associated with the details of surface charge distributions and retarded polarization effects²² are ignored. Nonetheless, in a recent paper, we showed that a similar pair average model approach²³ yielded results very similar to those of a more rigorous treatment,²⁴ even for the case of spheres in contact. Because the particles involved in that comparison were considerably larger than those discussed this study, we expect our results here to be reasonably accurate.

Random Pair Particles

Dispersions of nonspherical nanoparticles exhibit extinction spectra that contain contributions from each unique polarization axis. For nanoparticle pair dispersions, the general expressions for absorption and scattering cross sections should reflect an average of the principal axis pair average polarizabilities:

$$C_{\text{abs}} = k \text{Im} \left\{ \frac{1}{3} \langle \alpha_a \rangle + \frac{1}{3} \langle \alpha_b \rangle + \frac{1}{3} \langle \alpha_c \rangle \right\} \quad (12)$$

$$C_{\text{sca}} = \frac{k^4}{6\pi} \left(\frac{1}{3} \langle \alpha_a \rangle^2 + \frac{1}{3} \langle \alpha_b \rangle^2 + \frac{1}{3} \langle \alpha_c \rangle^2 \right) \quad (13)$$

For a rod pair aligned end-to-end, two of the three orientations are identical and will show identical responses to the electric field (Figure 3). This implies that the polarizability parallel to the b and c axes are the same ($\langle \alpha_b \rangle = \langle \alpha_c \rangle$). To calculate the average extinction of these random pairs, eqs 12 and 13 reduce to

$$C_{\text{abs}} = k \text{Im} \left\{ \frac{1}{3} \langle \alpha_a \rangle + \frac{2}{3} \langle \alpha_b \rangle \right\} \quad (14)$$

$$C_{\text{sca}} = \frac{k^4}{6\pi} \left(\frac{1}{3} \langle \alpha_a \rangle^2 + \frac{2}{3} \langle \alpha_b \rangle^2 \right) \quad (15)$$

It is also of interest to model random pair particles aligned in a side-to-side orientation (Figure 4). In this particle alignment, none of the three axes have identical depolarization and geometric factors. The b and c axes share an identical depolarization factor, L_x , because of particle shape considerations. However unlike the end-to-end alignment, they have different

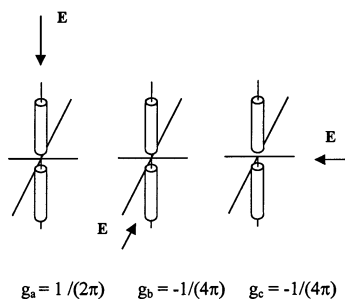


Figure 3. Schematic diagram of a rod pair oriented end-to-end and the associated orientation factor, g , for each electric field direction. The pair polarization responses of two of the three orientations are identical with respect to the incident electric field.

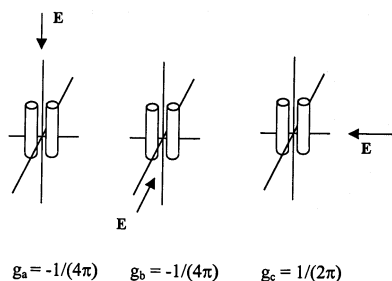


Figure 4. Schematic diagram of a rod pair oriented side-to-side and the associated orientation factor, g , for each electric field direction. The pair polarization response of each of the three orientations is unique with respect to the incident electric field.

mutual orientation factors (g) because the induced dipoles are in one case interacting side-to-side and in the other end-to-end. Therefore, when calculating an average random collection of particle pairs oriented side-to-side, there are three pair average polarizability conditions that must be taken into account. An extinction spectrum is calculated by substituting these values into eqs 12 and 13 and summing them to yield C_{ext} using eq 6.

In the experimental context, it would be reasonable for a single solution to have a combination of random pair particles with side-to-side alignment (eqs 12 and 13), and end-to-end alignment (eqs 14 and 15), along with free particles (eqs 4–6). It is also reasonable to anticipate that certain assays might be based on pair particles of mixed shapes (e.g., rod–sphere pairs). The theoretical treatment outlined above can be easily applied to such complex systems simply by using the appropriate depolarization factors (for particle shape) and g factors (for orientation), and coadding the C_{ext} functions according to the population fraction of each type of particle or paired structure present in the system.

Results and Discussion

Rod–Rod Interactions. Figure 5 shows the quasistatic limit simulation of two 5 nm radius spheres interacting at various distances. Optical data for gold were taken from Johnson and Christy²⁵ and the host refractive index was assumed to be 1.33. At a large center-to-center distance separation, there is no significant particle interaction and the metal spheres act independently, as displayed by the expected 524 nm resonance peak. As the particles are brought together until they are touching ($d_{12} = 10$ nm), the plasmon resonance peak red shifts to 532 nm. As the spheres interact and the pair qualitatively appears to be more rodlike, the effective aspect ratio (a/b) increases. As the semimajor axis a increases in length, the depolarization factor L_a (eq 2) decreases, resulting in an increase

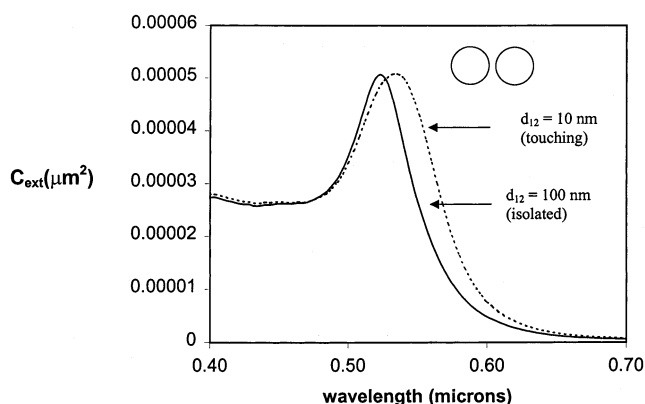


Figure 5. Calculated spectra of two spheres ($a = b = 5$ nm) with $d_{12} = 100$ nm (isolated) and with $d_{12} = 10$ nm (touching).

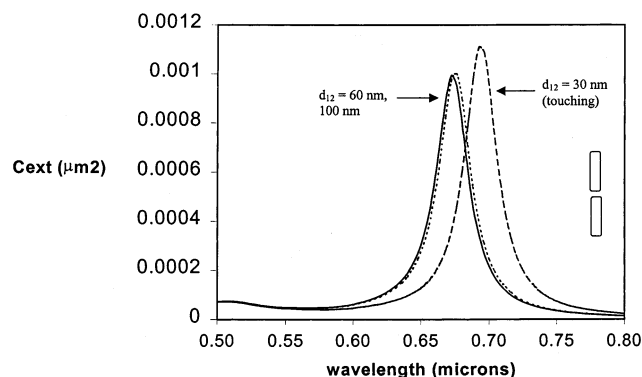


Figure 6. Calculated spectra of two medium length rods ($a = 15$ nm, $b = 5$ nm) interacting end-to-end at $d_{12} = 30$ nm (touching), 60 nm, and 100 nm (isolated).

in κ . Because the plasmon resonance condition is defined by the condition

$$\epsilon'_m = -\kappa\epsilon'_h \quad (16)$$

and because ϵ'_m for free electron metals becomes increasingly negative with increasing wavelength, an increase in κ will lead to a red shift in λ_{max} . In any case, the spectra shift for paired gold particles is relatively small.

Work has been previously done to model interacting end-to-end rods, and it has been shown that only slight red shifts in the λ_{max} peak are observed²³ as the rods are brought close enough to interact. A simulated example of end-to-end interacting rods is shown in Figure 6 ($a = 15$ nm, $b = 5$ nm). On the basis of the same reasoning as that for the sphere case, a red shift is expected as the rods come into contact via their long axes. However, like paired spheres, the peak shift associated with rods interacting end-to-end is not dramatic.

Figure 7 shows the simulated optical spectra for a side-to-side rod–rod pair particle at various distances. Figure 7A shows the interaction between two short rods of equal dimensions ($a = 10$ nm, $b = 5$ nm). When the particles are noninteracting ($d_{12} = 100$ nm), a long axis peak is observed at 590 nm with a short axis shoulder at 515 nm. These results are consistent with isolated rods. As they are brought closer together ($d_{12} = 20$ nm), the long axis peak blue shifts to 580 nm, while the short axis peak becomes less prominent. Once the particles are touching ($d_{12} = 10$ nm), the major peak blue shifts to 540 nm and only one broad peak is observed. The electric field interacts

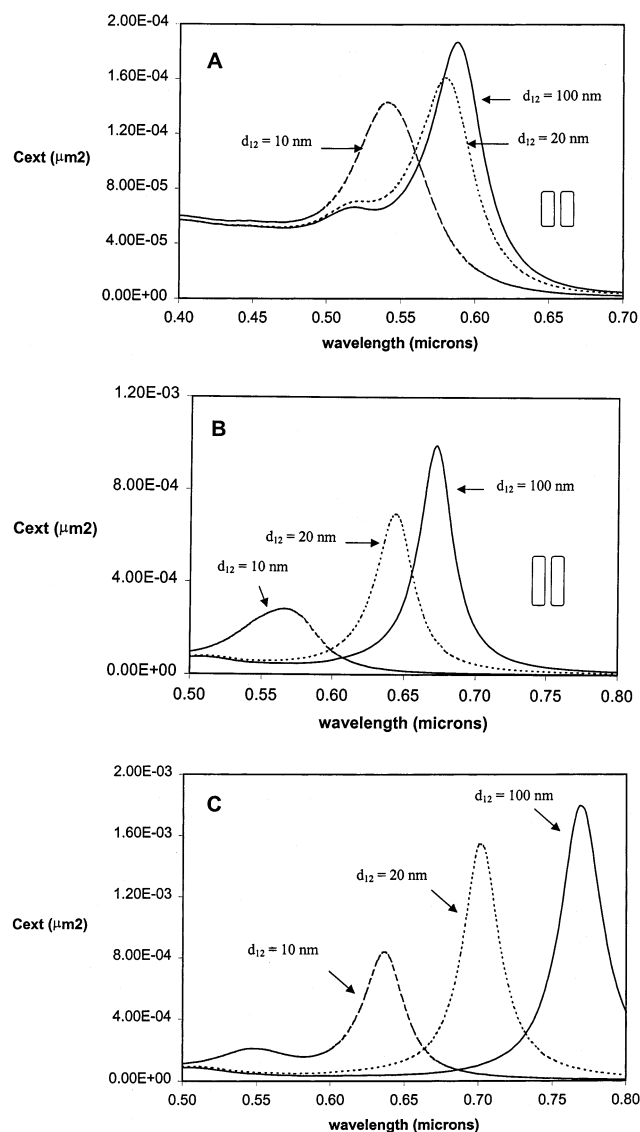


Figure 7. Calculated spectra of two rods interacting side-to-side at varying d_{12} lengths of 10, 20, and 100 nm with different lengths: (A) short rods ($a = 10$ nm, $b = 5$ nm); (B) medium rods ($a = 15$ nm, $b = 5$ nm); (C) long rods ($a = 20$ nm, $b = 5$ nm).

with these two rod particles almost as if they were a single spherical particle, resulting in a single resonance peak at 540 nm.

Figure 7B shows the simulated spectra for a medium length rod–rod pair ($a = 15$ nm, $b = 5$ nm) interacting side-to-side. In this case, the increased length of the rods (or increased κ) causes the long axis peak to be most prominent. When the particles are isolated ($d_{12} = 100$ nm), the long axis peak is at 670 nm with a short axis peak around 510 nm. As the particles are brought closer together ($d_{12} = 20$ nm), the particles begin to interact and a blue shift of the main resonance band to 640 nm is observed with negligible change to the short wavelength peak. Finally, as the particles are brought into intimate contact ($d_{12} = 10$ nm), a single broad peak appears centered at 565 nm and diminished in intensity.

Figure 7C shows the simulated spectra for two long rods ($a = 20$ nm, $b = 5$ nm). The isolated particles show a 767 nm prominent long axis peak and a negligible short axis shoulder. As the particles are brought closer together, the long axis peak blue shifts to 695 nm. Once the particles are touching, the long axis peak blue shifts to 637 nm with additional influence by the 545 nm short axis peak.

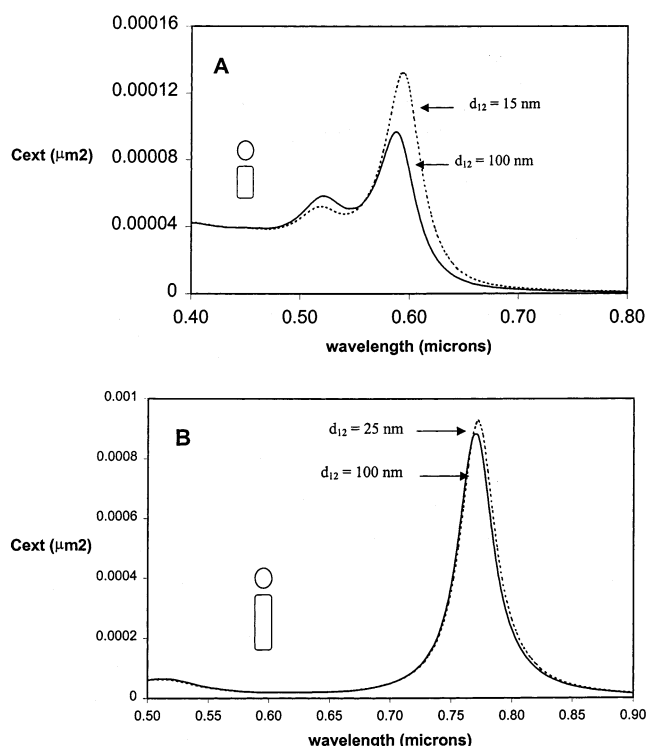


Figure 8. Calculated spectra of rod–sphere pairs with axial interaction at d_{12} values shown on curves: (A) short rod ($a = 10$ nm, $b = 5$ nm) and sphere ($a = b = 5$ nm); (B) long rod ($a = 20$ nm, $b = 5$ nm) and sphere ($a = b = 5$ nm).

Rod–Sphere Interactions. Figure 8 shows calculated spectra of sphere-to-rod end interactions over varying distances. For pairs involving low aspect ratio rods ($a = 10$ nm, $b = 5$ nm), decreasing d_{12} results in an appreciable red shift of the plasmon resonance maximum (Figure 8A). However, as the rod aspect ratio increases, the effect of association with a sphere is diminished (Figure 8B).

Figure 9A shows the spectrum resulting from the interaction between a short rod ($a = 10$ nm, $b = 5$ nm) and a small sphere ($a = b = 5$ nm) in which the sphere approaches in lateral fashion. The isolated particles ($d_{12} = 100$ nm) show their expected resonance peaks of 524 nm for the sphere and 585 nm for the rod. At a distance of 20 nm apart, the two particles slightly interact, and a decrease in the long wavelength peak is complemented by an increase in the short wavelength peak. Once in intimate contact, both sphere and rod peaks red shift to 550 and 610 nm, respectively.

Figure 9B shows the interaction of a medium rod ($a = 15$ nm, $b = 5$ nm) and a sphere ($a = b = 5$ nm). At $d_{12} = 100$ nm, the longitudinal resonance of the rod can be seen near 665 nm, and a shorter wavelength band near 520 nm which is the sum of the rod short axis and sphere resonances. At $d_{12} = 20$ nm, the spectral changes are insignificant. However, as the particles are brought into contact, both the long and short wavelength bands red shift. The same trends can be observed in Figure 9C, which depicts the effects of the association of a long rod ($a = 20$ nm, $b = 5$ nm) and sphere. At least for pairs in which the sphere radius is comparable to that of the rod, it appears that interactions are manifest in the spectra only at small d_{12} .

Mixtures in Solution. Figure 10 summarizes the spectral changes accompanying end-to-end and side-to-side interactions for a pair of rods (each of dimensions $a = 15$ nm, $b = 5$ nm). It is clear that side-to-side interactions of two rods or a pair consisting of a rod and a sphere yield dramatic spectral changes

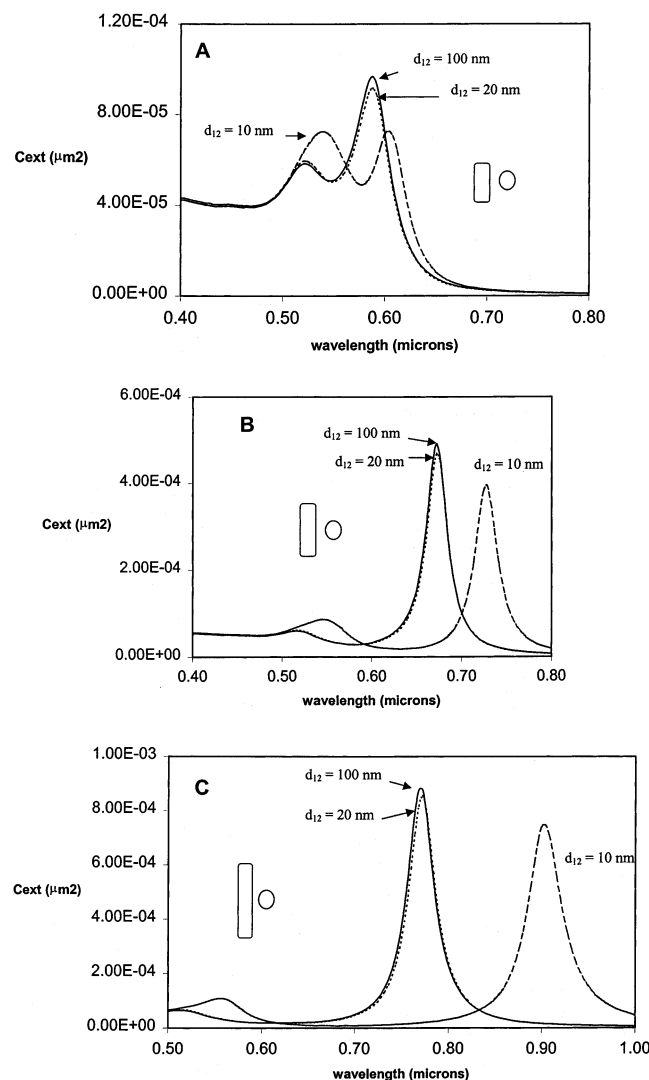


Figure 9. Calculated spectra of a side-to-side interacting sphere ($a = b = 5$ nm) and rod of different lengths at varying d_{12} lengths of 10, 20, and 100 nm: (A) short rods ($a = 10$ nm, $b = 5$ nm); (B) medium rods ($a = 15$ nm, $b = 5$ nm); (C) long rods ($a = 20$ nm, $b = 5$ nm).

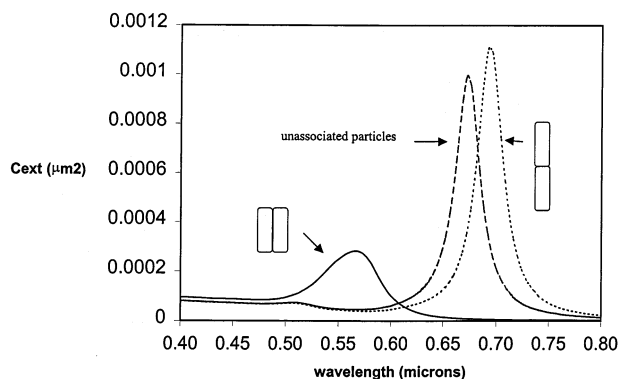


Figure 10. Spectra of rod pairs ($a = 20$ nm, $b = 5$ nm): (—) side-to-side, (---) end-to-end, and (· · ·) noninteracting.

(relative to the spectra of noninteracting particles), at least at this simple level of theory. A straightforward explanation of this observation is that in side-to-side orientations involving high aspect ratio particles, the mutual separation distance d_{12} between the center of the two dipoles is smaller than in the end-to-end configuration. Thus, the electric fields \mathbf{E}_1 and \mathbf{E}_2 experienced

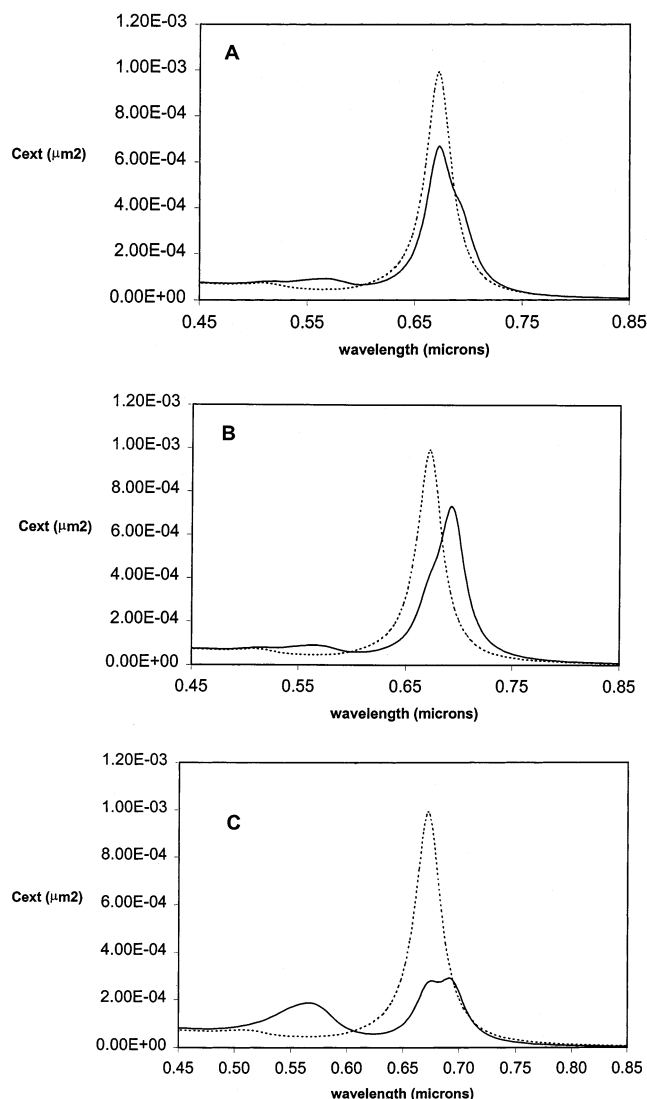


Figure 11. Calculated spectra for possible experimental scenarios with varying percentages of rod aggregation (—) oriented side-to-side and end-to-end in comparison to (---) free particles in solution for rod dimensions of $a = 15$ nm and $b = 5$ nm: (A) 60% free, 20% side-to-side, 20% end-to-end; (B) 20% free, 20% side-to-side, 60% end-to-end; (C) 20% free, 60% side-to-side, 20% end-to-end.

by each particle contain a higher contribution from the induced dipole of the other member of the pair.

Experimentally, it is unlikely that all of the nanoparticles in solution will align in pairs with the same orientation. By varying the percentages of particle pairs aligned end-to-end or side-to-side and by allowing for some free particles in solution, we can anticipate several nanoparticle scenarios that may be encountered in an assay protocol. In Figure 11, a comparison is made between nonassociated, randomly oriented rod particles and different combinations of oriented particle pairs. All of the spectra in Figure 11 are linear combinations of the spectra shown in Figure 10. In Figure 11A, the majority (60%) of the particle pairs are unassociated and paired species oriented side-to-side and end-to-end each represent 20% of the total population. For both the completely unassociated sample and the sample containing some associated particles, two major peaks can be observed. In the spectrum representing the mixed solution, the short axis peak is red-shifted from that of the free solution. The long axis peak of the mixture shows the slight growth of a red-shifted shoulder feature. Figure 11B examines the scenario in which the majority of particles are paired in an end-to-end

orientation. The spectrum of the sample containing associated particles shows two red-shifted peaks ($\lambda_{\text{max}} = 565$ and 695 nm) relative to that of the unassociated sample ($\lambda_{\text{max}} = 510$ and 670 nm). Finally, Figure 11C depicts a scenario where the sample contains a majority of side-to-side associated pairs. In this case, there are dramatic differences between the sample containing associated particles and that containing unassociated particles. In the mixed system, the overall extinction intensity is diminished ca. 70% and the spectrum now shows three major peaks (at 565 , 675 , and 695 nm).

The selection of the percentage of each particle pair type in the above examples is certainly arbitrary but nonetheless illustrates possibility for new metal nanoparticle based assays. Whereas the linking of nanospheres in solution always results in a red shift and broadening of the plasmon resonance band, the association of rods can result in either a red or blue shift, depending on mutual orientation. If future synthetic methods are developed for regio-specific modification of the nanoparticle surface (e.g., one type of probe group at the rod ends and another along the sides), then perhaps rodlike metal nanoparticles may allow for the simultaneous analysis of more than one target species.

Conclusions

A simple quasistatic limit treatment was used to calculate the plasmon resonance spectra of gold nanoparticle pairs in which at least one pair member was rodlike. The nature of the spectral change as the distance between pair members decreases depends on whether the mutual orientation is lateral (side-to-side) or axial (end-to-end). In general, the spectral consequence of end-to-end interactions is a red shift of the longitudinal rod mode. This red shift becomes less apparent as the aspect ratio of the rod(s) increases. Conversely, side-to-side interactions of nanorods lead to a blue shift in the main plasmon resonance band with the corresponding growth in the short axis band.

Lateral rod-sphere interactions do not result in significant spectral changes unless d_{12} is very small. Upon contact, the pair spectrum retains dominant long and short wavelength bands, both of which are red-shifted relative to the two bands of the noninteracting particle spectrum.

Should rod-rod pairs be used in nanometal particle based assays of biomolecules or other target species, the quasistatic model presented here predicts that side-to-side (lateral) interactions will likely provide more sensitivity than interparticle links that lead to end-to-end (axial) interactions.

Acknowledgment. This material is based on work supported by the National Science Foundation under Grant DMR 9625151. M.G. also acknowledges the support of the Georgetown University Department of Chemistry.

References and Notes

- (1) Elghanian, R.; Storhoff, J. J.; Mucic, R. C.; Letsinger, R. L.; Mirkin, C. A. *Science* **1997**, 277, 1078–1080.
- (2) Storhoff, J. J.; Elghanian, R.; Mucic, R. C.; Mirkin, C. A.; Letsinger, R. L. *J. Am. Chem. Soc.* **1998**, 120, 1959–1964.
- (3) Demers, L. M.; Mirkin, C. A.; Mucic, R. C.; Reynolds, R. A., III; Letsinger, R. L. *Anal. Chem.* **2000**, 72, 5535–5541.
- (4) Taton, T. A.; Mirkin, C. A.; Letsinger, R. L. *Science* **2000**, 289, 1757–1760.
- (5) Reynolds, R. A., III; Mirkin, C. A.; Letsinger, R. L. *Pure Appl. Chem.* **2000**, 72, 229–235.
- (6) Reynolds, R. A., III; Mirkin, C. A.; Letsinger, R. L. *J. Am. Chem. Soc.* **2000**, 122, 3795–3796.
- (7) Schmitt, J.; Machtle, P.; Eck, D.; Mohwald, H.; Helm, C. A. *Langmuir* **1999**, 15, 3256.
- (8) Preston, C. K.; Moskovits, M. *J. Phys. Chem.* **1988**, 92, 2957.
- (9) Tierney, M. J.; Martin, C. R. *J. Phys. Chem.* **1989**, 93, 2878.
- (10) Foss, C. A., Jr.; Hornyak, G. L.; Stockert, J. A.; Martin, C. R. *J. Phys. Chem.* **1994**, 98, 2963.
- (11) Al-Rawashdeh, N. R.; Sandrock, M. L.; Seugling, C. J.; Foss, C. A., Jr. *J. Phys. Chem. B* **1998**, 102, 361.
- (12) Sandrock, M. L.; Pibel, C. D.; Geiger, F. M.; Foss, C. A., Jr. *J. Phys. Chem. B* **1999**, 103, 2668.
- (13) van der Zande, B. M. I.; Bohmer, M. R.; Fokkink, L. G. J.; Schonenberger, C. *J. Phys. Chem. B* **1997**, 101, 852.
- (14) van der Zande, B. M. I.; Bohmer, M. R.; Fokkink, L. G. J.; Schonenberger, C. *Langmuir* **2000**, 16, 451.
- (15) Yu, Y. Y.; Chang, S. S.; Lee, C. L.; Wang, C. R. C. *J. Phys. Chem. B* **1997**, 101, 6661.
- (16) Chang, S. S.; Shih, C. W.; Chen, C. D.; Lai, W. C.; Wang, C. R. C. *Langmuir* **1999**, 15, 701.
- (17) It should be noted that current metal nanosphere based assays derive their sensitivity from the analyte-induced formation of large aggregates of nanoparticles and not simple pairs. Cooperative effects in the thermal dissociation of these aggregates lead to very abrupt spectral changes as the temperature is increased, which in turn are highly advantageous in the analysis of complimentary DNA base pair sequences (C. A. Mirkin, personal communication).
- (18) van de Hulst, H. C. *Light Scattering by Small Particles*; Dover: New York, 1981.
- (19) Bohren, C. F.; Huffman, D. R. *Absorption and Scattering of Light by Small Particles*; John Wiley: New York, 1983.
- (20) Kriebig, U.; Vollmer, M. *Optical Properties of Metal Clusters*; Dover: New York, 1981.
- (21) Halliday, D.; Resnick, R. *Fundamentals of Physics*, 2nd ed.; John Wiley and Sons: New York, 1981.
- (22) Granquist, C. G.; Hunderi, O. *Phys. Rev. B* **1977**, 16, 1353.
- (23) Sandrock, M. L.; Foss, C. A., Jr. *J. Phys. Chem. B* **1999**, 103, 11398.
- (24) Jensen, T.; Kelly, L.; Lazarides, A.; Schatz, G. C. *J. Cluster Sci.* **1999**, 10, 295.
- (25) Johnson, P. B.; Christy, R. W. *Phys. Rev. B* **1972**, 6, 4370.